

Numerical simulation of two-phase slug flows in horizontal pipelines: A 3-D smoothed particle hydrodynamics application

Massoud Rezavand^{a,*}, Xiangyu Hu^a

^a*Department of Engineering Physics and Computation, TUM School of Engineering and Design, Technical University of Munich, 85748 Garching, Germany*

Abstract

A fundamental difficulty of studying gas-liquid pipe flows is the prediction of the occurrence and characteristics of the slug flow regime, which plays a crucial role in the safety design of oil pipelines. Current empirical methods and one-dimensional computational models only achieve limited success. While 3-D numerical simulations are highly recommended, they have been very seldom used. We perform 3-D Lagrangian numerical simulations of gas-liquid pipe flows, and focus on the interfacial instabilities leading to slug formation. We adapt an existing multi-phase smoothed particle hydrodynamics (SPH) method based on a Riemann solver to achieve an efficient solver with no dependency on empirical correlations. To realize the high inlet velocities of gas and liquid an in- and outlet boundary condition is presented. The results are validated against existing experimental data, numerical simulations and analytical solutions. Multiple gas-liquid pipe flow patterns are predicted, namely, smooth stratified, stratified wavy, bubble flow, slug flow and bubble flow. Several principle characteristics of slug flows, e.g., pressure gradient, slug development and slug frequency are analyzed.

Keywords: Intermittent flows, Multi-phase, Pipe flows, Slug flows, Smoothed Particle Hydrodynamics

*Corresponding author

Email addresses: massoud.rezavand@tum.de (Massoud Rezavand), xiangyu.hu@tum.de (Xiangyu Hu)

1. Introduction

Gas-liquid multi-phase flows in piping systems are ubiquitous in a wide range of industrial applications, e.g., nuclear power plants, crude oil mixed transportation, condensation, distillation towers and filling or emptying operations among others. At high flow rates, this category of flows can often demonstrate flow characteristics that might play a destructive role in pipelines. For this reason it is of high importance to study and understand them well, in order to prevent the undesired phenomena [1, 2].

Given various physical conditions, such as flow rate, pipe diameter and inclination and mixture fractions, multi-phase pipe flows experience significantly different characteristics and flow regimes. One of the most common flow patterns that occurs in petroleum and chemical industries is the formation and migration of liquid slugs in piping systems. For instance, the flow conditions governing most the transportation processes in oil wells lie within the range of slug flow regime [3]. A fundamental difficulty of studying such flows is on predicting the occurrence and characteristics of the flow regimes [4, 5]. For gas-liquid pipe flows, in particular, such difficulty is on predicting when the slug flow regime occurs and how it is characterized, which are highly relevant to the safety design of the oil pipelines. Several flow regime prediction models have been developed to describe two-phase pipe flow patterns and flow transitions, which are either empirical or based on experimental observations (e.g., [6, 7, 8, 9]). Despite being substantially useful and widely applied for designing industrial applications, these models are not adequate for a complete flow definition, as they do not represent the interaction of various forces involved in the flow.

In another approach, numerous studies have been dedicated to develop and apply one-dimensional (1-D) thermal hydraulic system codes to represent flow patterns and transitions (e.g., [10, 11, 12, 13, 14]). 1-D solvers are useful in predicting the overall behavior of the process systems, however, they consider

major simplifications and are thus not appropriate for comprehensive flow analysis. They generally assume a fully developed flow and neglect details of interfacial area, mass transfer, viscous energy dissipation and turbulence effects and treat the flow governing equations in a simplified manner. For this reason, some studies have attempted to couple such models with more comprehensive fluid flow solvers to fill the gap (see e.g., [15, 16, 17]).

Intermittent flows have also been extensively studied experimentally considering various aspects of the problem (e.g., [18, 19, 20]). However, experimental techniques are costly, resource-intensive and not applicable for all full-scale piping systems. Thanks to modern high performance computers, computational fluid dynamics (CFD) methods have emerged as promising tools to study multi-phase pipe flows (see e.g., [18, 20, 21]). In order to simulate slug flow problems, the main challenge of the traditional Eulerian mesh-based methods is to deal with its multi-phase nature and the interfacial complexities. For instance, the volume of fluid (VOF) approach has been implemented in commercial packages by Taha and Cui [22] and Al-Hashimy et al. [23] to simulate two-phase slug flows in capillaries and pipelines, respectively. The Level-set (LS) and lattice-Boltzmann (LB) methods were also employed to study slug flows in microchannels for the applications in microfluidic devices [24, 25]. Computationally more expensive methods, e.g., direct numerical simulations (DNS) have also been used for the simulation of two-phase slug flows in inclined pipes. Xie et al. [26] also compared two-dimensional (2-D) results with three-dimensional (3-D) ones in their DNS studies and concluded that there are differences between 2-D and 3-D simulations in terms of circulation dynamics and vorticity generation.

In recent decades, Lagrangian mesh-free methods have emerged as an attractive alternative for mesh-based methods in the simulation of multi-phase flows (see e.g., [27, 28, 29]). As an advanced member of this class of methods, smoothed particle hydrodynamics (SPH) is a fully Lagrangian particle-based method that has been proposed in late 1970s for astrophysics. SPH has already been successfully used for a wide range of theoretical and engineering problems, ranging from free-surface flows to human cardiac function simulations (see e.g.,

[30, 31, 32, 33]) Owing to its Lagrangian nature, SPH naturally realizes the multi-phase interface with no need for an additional algorithm. These peculiarities nominates SPH as a promising choice for simulating multi-phase pipe flows and has been already employed for slug flow simulations (e.g., [17, 34, 35]).

Although the previous SPH simulations of intermittent pipe flows have shed light on the nature of slugging from a Lagrangian point of view, those studies are limited to 1-D or 2-D frameworks. To the best of our knowledge, the 3-D Lagrangian numerical investigation of slug flows is still unaddressed. As Xie et al. [26] concluded, 3-D simulations of slug flows are of importance for a comprehensive representation of the flow structures. On the other hand, as a well-established turbulence model has not yet been presented for the SPH formulation in industrial scales, it is important to carry out 3-D SPH simulations in order to capture the large vortices, relying on the inherent large-eddy simulation (LES) turbulence mechanisms of SPH [36]. Cleary and Monaghan [37] proposed that dissipation mechanisms exist at the sub-particle scales of the SPH scheme that cause energy dissipation, thereby preventing excessive energy accumulation at the larger scales. Ting et al. [38] and Ghasemi et al. [36] confirmed this proposal with their SPH simulations of turbulent flows and considered SPH as a natural LES method. Furthermore, they realized that for more accurate results 3-D computations should be conducted.

The above considerations are the motivations of the present study to perform robust 3-D simulations of gas-liquid pipe flows within the fully Lagrangian framework of the SPH method. The application of SPH for such an industrial problem will also address the fifth grand challenge of the SPH method [39]: applicability to industry. In addition, we aim at presenting a numerical framework with no empirical dependency with a relatively good computational efficiency to fill the gap highlighted by the comprehensive studies of Mohammed et al. [40]. To achieve these goals, we implemented our methodologies in the open-source SPHinXsys library [41] being available with accompanying information at <https://www.sphinxsys.org>.

We firstly present an in- outflow boundary condition implemented in the

open-source SPHinXsys library [31], which enables us to apply desired inlet velocity of both gaseous and liquid phases. Secondly, the accuracy and convergence of the proposed numerical framework is quantitatively verified in comparison with analytical solutions. We next validate the presented method against experimental observations in five different gas-liquid pipe flow regimes. The initiation of the first slug at the entrance of the pipe has also been addressed here. Finally, various characteristics of a slug flow regime in a horizontal pipe is investigated, namely, pressure and velocity distribution throughout the pipe, development of a slug along the pipe and slug frequency. The obtained results by the presented SPH method are further compared with the available data sets in the literature and the method demonstrates good accuracy and robustness.

2. Numerical method

Intermittent two-phase flows, e.g., slug flow, are typically considered as two-phase flows with large density ratio, i.e., $\rho_l/\rho_g \gg 1$, where ρ_l and ρ_g represent the densities of liquid and gaseous phases. Such problems have been investigated in our previous works in an inviscid regime [30, 42]. With the consideration of the viscous effects for slug flows, the mass and momentum conservation equations can be written respectively as

$$\frac{d\rho}{dt} = -\rho\nabla \cdot \mathbf{v}, \quad (1)$$

$$\frac{d\mathbf{v}}{dt} = -\frac{1}{\rho}\nabla p + \nu\nabla^2\mathbf{v} + \mathbf{g}, \quad (2)$$

where d/dt is the Lagrangian derivative, ρ the density, \mathbf{v} the velocity, p the pressure, ν the kinematic viscosity and \mathbf{g} the gravitational acceleration. To close the system in a weakly compressible SPH (WCSPH) framework, pressure is estimated from density via an artificial equation of state (EoS), within the weakly compressible framework. Here, we use a simple linear equation for both the heavy and light phases

$$p = c^2(\rho - \rho_0), \quad (3)$$

where c and ρ_0 are the artificial speed of sound and the initial reference density. Here, we assume that the speed of sound is constant and we set $c = 10U_{max}$, where U_{max} denotes the maximum anticipated velocity of the flow. Following the methodology presented in Ref. [30] we use the same value of c for both heavy and light phases, which leads to larger time-step sizes and thereby higher computational efficiency for the resource-intensive 3-D computations of the simulations presented in this work.

In order to cope with the complex two-phase phenomena in intermittent flows we adapt the method presented in Ref. [30, 42]. The particle summation formulation [43] is used to realize the mass conservation principle for the gaseous phase

$$\rho_i = m_i \sum_j W_{ij}, \quad (4)$$

where m_i denotes the mass of particle i and the smoothing kernel function $W(|\mathbf{r}_{ij}|, h)$ is simply substituted by W_{ij} , with $\mathbf{r}_{ij} = \mathbf{r}_i - \mathbf{r}_j$ being the displacement vector between particle i and j and h the smoothing length, respectively. The discretized form of the continuity equation is, on the other hand side, employed for the liquid phase

$$\frac{d\rho_i}{dt} = \rho_i \sum_j \frac{m_j}{\rho_j} \mathbf{v}_{ij} \cdot \nabla_i W_{ij} = 2\rho_i \sum_j \frac{m_j}{\rho_j} (\mathbf{v}_i - \bar{\mathbf{v}}_{ij}) \cdot \nabla_i W_{ij}, \quad (5)$$

where $\mathbf{v}_{ij} = \mathbf{v}_i - \mathbf{v}_j$ is the relative velocity and $\bar{\mathbf{v}}_{ij} = \frac{\mathbf{v}_i + \mathbf{v}_j}{2}$ denotes the average velocity between particle i and j . Furthermore, the momentum conservation principle has been realized by the formulation presented in Ref. [43] excluding the artificial viscosity,

$$\frac{d\mathbf{v}_i}{dt} = -2 \sum_j m_j \frac{\bar{p}_{ij}}{\rho_i \rho_j} \nabla_i W_{ij} + 2 \sum_j \nu_i V_j \frac{\mathbf{v}_{ij}}{r_{ij}} \frac{\partial W_{ij}}{\partial r_{ij}} + \mathbf{g} \quad (6)$$

with $\bar{p}_{ij} = \frac{p_i + p_j}{2}$ being the average pressure between particle i and j , V the particle volume and $r_{ij} = |\mathbf{r}_i - \mathbf{r}_j|$.

2.1. WCSPH multi-phase Riemann solver for slug flow

In WCSPH methods based on a Riemann solver [44, 45, 30], an inter-particle Riemann problem is constructed along the unit vector $\mathbf{e}_{ij} = -\frac{\mathbf{r}_{ij}}{|\mathbf{r}_{ij}|}$ between the

interacting particles i and j by piecewise constant approximation as follows

$$\begin{cases} (\rho_L, U_L, p_L) = (\rho_i, \mathbf{v}_i \cdot \mathbf{e}_{ij}, p_i) \\ (\rho_R, U_R, p_R) = (\rho_j, \mathbf{v}_j \cdot \mathbf{e}_{ij}, p_j) \end{cases}, \quad (7)$$

The solution of the Riemann problem can be shown using a $x - t$ diagram, for which the readers are referred to Ref. [30] to see more details. For multi-phase flows with the same speed of sound across the interface, following Ref. [46], the intermediate velocity and pressure can be approximated as

$$\begin{cases} U^* = \bar{U} + \frac{p_L - p_R}{c(\rho_L + \rho_R)}, \\ p^* = \bar{P} + \frac{\rho_L \rho_R \beta (U_L - U_R)}{\rho_L + \rho_R}, \end{cases} \quad (8)$$

where $\bar{U} = (\rho_L U_L + \rho_R U_R)/(\rho_L + \rho_R)$ and $\bar{P} = (\rho_L p_R + \rho_R p_L)/(\rho_L + \rho_R)$.

For two-phase particle interactions with large density ratio, as in slug flow problems, Eq. (8) gives approximately the intermediate velocity from the heavy phase, which indicates that the light phase experiences the heavy phase as a moving wall boundary, and intermediate pressure from the light phase, which indicates that the heavy phase undergoes a free-surface-like flow with variable free-surface pressure [46]. Having the intermediate values determined from the solution of the Riemann problem, the mass and momentum conservation equations, i.e., Eqs. (5) and (6), can be rewritten as

$$\frac{d\rho_i}{dt} = 2\rho_i \sum_j \frac{m_j}{\rho_j} (\mathbf{v}_i - \mathbf{v}^*) \cdot \nabla_i W_{ij}, \quad (9)$$

$$\frac{d\mathbf{v}_i}{dt} = -2 \sum_j m_j \frac{p^*}{\rho_i \rho_j} \nabla_i W_{ij} + 2 \sum_j \nu_i V_j \frac{\mathbf{v}_{ij}}{r_{ij}} \frac{\partial W_{ij}}{\partial r_{ij}} + \mathbf{g} \quad (10)$$

where $\mathbf{v}^* = U^* \mathbf{e}_{ij} + (\bar{\mathbf{v}}_{ij} - \bar{U} \mathbf{e}_{ij})$ and $\bar{\mathbf{v}}_{ij} = (\rho_i \mathbf{v}_i + \rho_j \mathbf{v}_j)/(\rho_i + \rho_j)$, which is a density-weighted average velocity between particle i and j .

2.2. Gas-liquid pipe flow considerations

Given gas and liquid phases, pipe geometry and inclination angle, the flow is determined by the superficial velocities v_{sg} and v_{sl} . These properties are given

by the gas and liquid volumetric flow rates Q_g and Q_l , respectively

$$v_{sg} = \frac{Q_g}{A} = v_g \alpha_g, \quad v_{sl} = \frac{Q_l}{A} = v_l \alpha_l, \quad \alpha_g + \alpha_l = 1 \quad (11)$$

where v_g and v_l are the gas and liquid velocities, respectively, A is the cross-section area of the pipe and α_g and α_l are the volumetric gas fraction and liquid fraction, or holdup, respectively. The mixture velocity is then defined by the gas and liquid superficial velocities as

$$v_m = \frac{Q}{A} = v_{sg} + v_{sl} \quad (12)$$

where Q is the overall flow rate.

2.3. Boundary conditions

2.3.1. Solid wall

In the present study, we use fixed dummy particles to impose the solid wall condition as proposed in Ref. [30] and further generalized for multi-phase flows in Ref. [42]. To realize the fluid-wall interactions a Riemann problem is constructed between particles of fluids and wall dummy particles, as for fluid-fluid interactions (see Section 2.1). However, the intermediate pressure value is obtained as

$$p^* = \frac{\rho_f p_w + \rho_w p_f}{\rho_f + \rho_w}, \quad (13)$$

where subscripts f and w denote fluid and wall, respectively, to decrease the wall-induced numerical dissipation while the intermediate velocity value U^* is still obtained via Eq. (8), as for fluid-fluid interactions. Similar to Ref. [47], the pressure of wall dummy particles is calculated by the summation over all contributions of the neighboring fluid particles as

$$p_w = \frac{\sum_f \frac{p_f}{\rho_f} W_{wf} + (\mathbf{g} - \mathbf{a}_w) \sum_f \mathbf{r}_{wf} W_{wf}}{\sum_f \frac{W_{wf}}{\rho_f}}. \quad (14)$$

where \mathbf{a}_w denotes the wall acceleration. It is worth noting that by introducing ρ_f into Eq. (14) the contribution of liquid particles in p_w at a triple point, where liquid, gas and solid particles meet, is vanishing. As also presented by Adami et al. [47], the density of wall dummy particles is obtained from pressure via Eq. (3).

2.3.2. In- and outflow

The in- and outflow boundary condition using the emitter technique offered by SPHinXsys has been discussed in detail by Zhang et al. [48]. In this section, we present another possibility in the library to implement this boundary condition using a transition area. As shown in Fig. 1, SPHinXsys considers a transition area, where the desired inlet velocity profile is applied on the particles. This implementation takes advantage of the cell-linked list constructed for neighbor search procedure, where the inlet and outlet areas, located within $2h$ from the domain edge, are marked as cells where the particles need to be generated (at inlet) or removed (at outlet). In this manner, a periodic boundary condition is realized, which is essential for an in- and outflow condition. The appropriate physical variables for particles in the inlet and outlet areas are then analytically applied and next extrapolated from within the flow domain, considering the smoothing kernel support radius [49]. As the inlet velocity magnitude in the test cases presented herein are relatively high, to have a stable inlet area we define a minimum transition length of $20dx$, where dx is the initial particle spacing. The configuration of the transition area together with the periodic boundary condition inlet and outlet areas are then updated at every time step as discussed in Section 2.4.

2.4. Time integration

The time integration of the equations of motion in the present study employs the kick-drift-kick [50, 51] scheme. The first half-step velocity is obtained as

$$\mathbf{v}_i^{n+\frac{1}{2}} = \mathbf{v}_i^n + \frac{\delta t}{2} \left(\frac{d\mathbf{v}_i}{dt} \right)^n, \quad (15)$$

from which we obtain the position of particles at the next time step

$$\mathbf{r}_i^{n+1} = \mathbf{r}_i^n + \delta t \mathbf{v}_i^{n+\frac{1}{2}}. \quad (16)$$

With the updated flow states, the density of heavy-phase particles at the new time step is then calculated as

$$\rho_i^{n+1} = \rho_i^n + \delta t \left(\frac{d\rho_i}{dt} \right)^{n+\frac{1}{2}}, \quad (17)$$

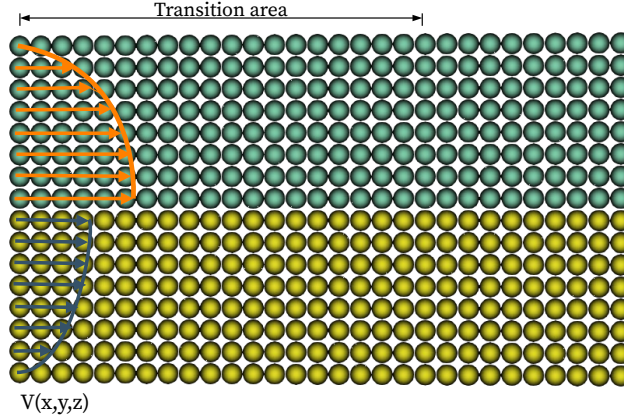


Figure 1: Schematic illustration of the in- and outlet boundary condition depicting different inlet velocity profiles for the gaseous (top) and liquid (bottom) phases together with the transition area. No-slip boundary condition is implemented on the surrounding solid walls.

where the time increment of density is approximated via Eq. (5). It is worth noting that the density of light phase particles at the new time step is obtained using the density summation equation, i.e. Eq. (4). With the new densities being calculated, the pressure of particles and the time increment of velocity, can be obtained. As a final step to calculate the physical properties of the inner particles, the velocity of particles is updated for the new time step as

$$\mathbf{v}_i^{n+1} = \mathbf{v}_i^{n+\frac{1}{2}} + \frac{\delta t}{2} \left(\frac{d\mathbf{v}_i}{dt} \right)^{n+1}. \quad (18)$$

In order to realize the in- and outlet boundary condition, the particle configuration at the inlet and outlet areas will be updated according to the marked cells and the parabolic inlet velocity profiles will be imposed. The analytical properties will be next extrapolated from the values within the flow domain. To guarantee the numerical stability, the time-step size is limited by the CFL condition

$$\delta t \leq 0.25 \left(\frac{h}{c + U_{max}} \right), \quad (19)$$

together with the body force and viscous conditions

$$\delta t \leq 0.25 \min \left(\sqrt{\frac{h}{|\mathbf{g}|}}, \frac{h^2}{\nu} \right). \quad (20)$$

3. Model validation

As the accuracy and robustness of the SPHinXsys library have been already demonstrated in various applications including fluid and solid dynamics [52, 53, 31], fluid structure interaction (FSI) [54, 55] and biomechanics [56, 32], in this section we consider two additional test cases, which showcase the ability of the library to capture the underlying physics of intermittent two-phase pipe flows. Firstly, we quantitatively verify the flow properties in the Hagen-Poiseuille problem as a classical 3-D internal viscous flow. Secondly, the SPH simulations of a two-phase flow of gas and water under different velocity conditions in a horizontal pipe are validated against experimental results carried out by Wu et al. [20].

3.1. Hagen-Poiseuille flow

Due to the shear phenomena in Poiseuille flows both in 2- and 3-D, these problems are proper test cases to verify the viscosity model employed in the present methodology against analytical solutions [57, 27]. The schematic of this problem is illustrated in Fig. 2. An incompressible liquid with a density of $\rho = 1000 \text{ kg.m}^{-3}$ is flowing in the x -direction of a cylindrical channel with a diameter of $d = 1 \text{ mm}$ and the flow is driven by a horizontal free-stream velocity of $U_{max} = 0.1 \text{ mm.s}^{-1}$. The dynamic viscosity of the liquid is $\mu = 0.001 \text{ mPa.s}$, which along with other physical properties determines the Reynolds number of the flow as $Re = 100$. In this section, the periodic and no-slip boundary conditions are used for wall and horizontal boundaries, respectively.

The velocity profile obtained from the single-phase SPH formulation presented in Section 2 are compared with the analytical solutions derived by Bird et al. [58] in Fig. 3a. As shown in the figure, the SPH simulation with an initial

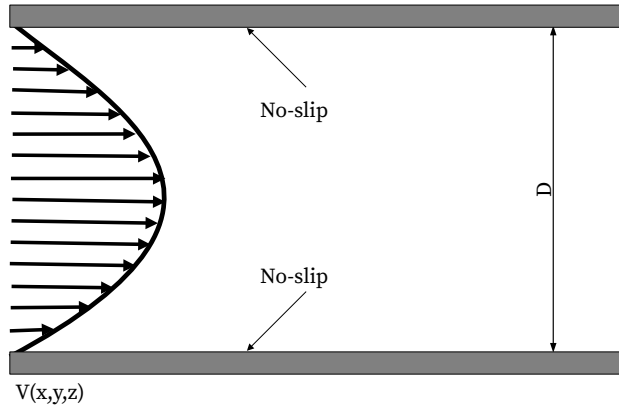


Figure 2: Schematic illustration of the 3-D Hagen-Poiseuille flow test case.

particle spacing of $dx = D/20$ demonstrates a close agreement with the analytical solution. To further evaluate the numerical aspects of the proposed method, Fig. 3b analyzes the convergence properties by the variation of the L_2 -norm of error [59] with respect to the particles resolution. As it can be observed, an approximately first-order convergence is obtained.

In order to investigate the viscous flow characteristics in more detail, 3-D SPH particle distribution and contours of the velocity magnitude with $dx = D/20$ are presented in Figs. 4a and 4b, respectively. The particle distribution and the velocity field both demonstrate a smooth behavior with no spurious quantities. Furthermore, the near wall velocity magnitude is noise-free, which demonstrates an accurate realization of the mass and momentum conservation equations and robust boundary condition implementations.

3.2. Gas-liquid multi-phase flow in a pipe under various velocity conditions

To validate the presented SPH method against experiments, we used the results obtained by Wu et al.[20]. The experimental apparatus is described in their work with all details. The apparatus uses a horizontal cylindrical tube with an inner diameter of 50 mm and a length of 13 m ($260D$). Gas (air) and liquid (water) enter the tube with constant flow rates through separated

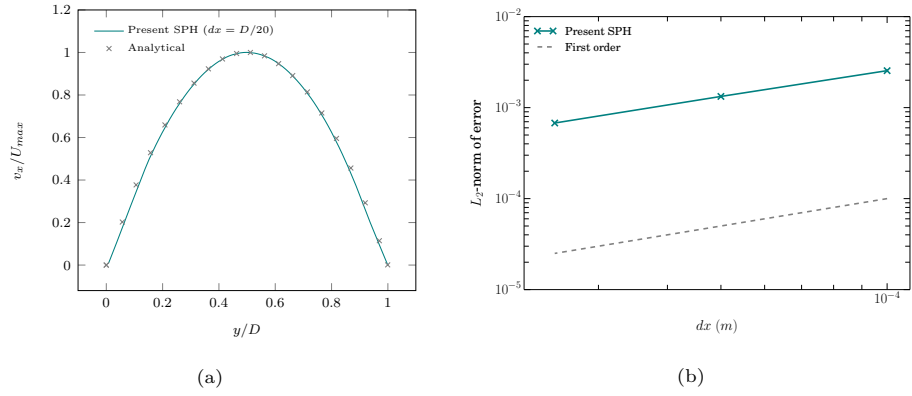


Figure 3: Hagen-Poiseuille flow: (a) Velocity profile obtained by the present SPH method in comparison with the analytical solution and (b) L_2 -norm convergence analysis at $t = 10$ s.

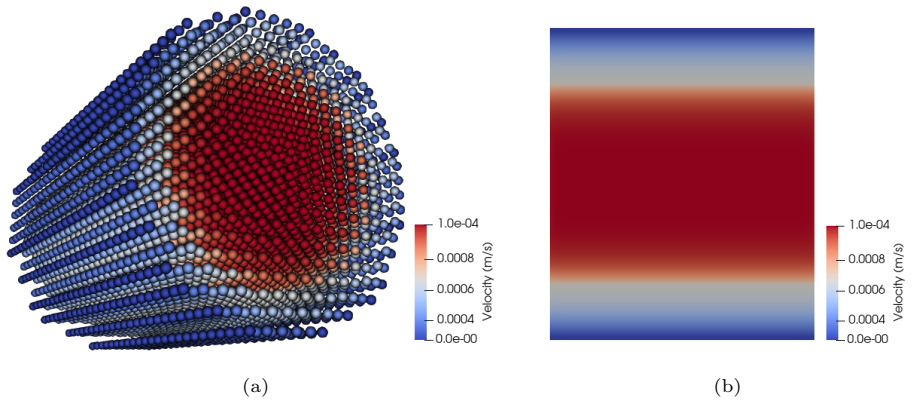


Figure 4: Hagen-Poiseuille flow: (a) 3-D SPH particle distribution with particles being scaled by their velocity magnitude and (b) a y -normal cross section of the velocity profile at the same time instant with $dx = D/20$.



Figure 5: Gas-liquid multi-phase flow in a horizontal pipe: Initial geometric configuration of the 3-D horizontal pipe. The upper half of the particles belong to the gaseous phase and the lower ones belong to the liquid phase.

Physical property	Gaseous phase	Liquid phase
Density ($\text{kg}\cdot\text{m}^{-3}$)	1.204	998.2
Dynamic viscosity (Pa.s)	1.837×10^{-5}	8.891×10^{-4}
Gravity ($\text{m}\cdot\text{s}^{-2}$)	9.81	9.81

Table 1: Physical properties of the light and dense fluids involved in the studied gas-liquid multi-phase flow cases in horizontal pipe and under various velocity conditions.

inlet cross-sections and mix by a stratified mixer with a length of 0.5 m at the inlet of the tube. The initial configuration of our SPH simulations is depicted in Fig. 5 and the physical properties of the gaseous and the liquid phases are summarized in Table 1. In order to have a more accurate understanding of the problem configuration, the schematic view of the problems is also shown in Fig. 6, where the position of the pressure sensors used in the next sections are clarified, as well.

Depending on the superficial velocity conditions, various flow patterns will develop for which the flow characteristics are summarized in Table 2. In this

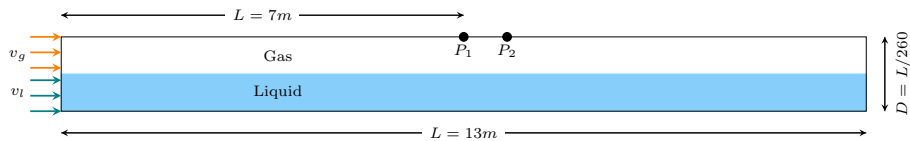


Figure 6: Gas-liquid multi-phase flow in a horizontal pipe: Schematic illustration of the problem. P_1 and P_2 show the location of the two sensors used for recording pressure signals.

ID	Flow pattern	v_{sg} (m.s ⁻¹)	v_{sl} (m.s ⁻¹)
SS	Smooth stratified	0.5	0.1
SW	Stratified wavy	2.5	0.1
BF1	Bubble flow	0.1	3.0
SF	Slug flow	5.0	1.0
BF2	Bubble flow	0.3	1.0

Table 2: Velocity condition and flow pattern description of the test cases presented in Fig. 7

section, we consider five different flow patterns according to the Mandhane flow pattern diagram [6] depicted by Wu et al., namely, smooth stratified (SS), stratified wavy (SW), bubble flow (BF1 and BF2) and slug flow (SF).

The obtained results by the presented SPH method has been compared to the experimental observations of Wu et al.[20] in Fig. 7. As it is can be observed, the overall flow regime has been reproduced by both SPH and OpenFOAM in comparison with the experiments, while discrepancies are present in such a complex multi-phase flow. It is also seen that some SPH particles from the gaseous phase have entered the liquid phase, which is due to the fact that no special multi-phase interface sharpening technique has been employed in the presented SPH method as explained in Ref. [30]. The present SPH simulations are in 3-D and with the large computational domain size in mind, we are dealing with a considerably large number of particle experiencing complex phenomena. For this reason, the resolution of the SPH model is lower that of the OpenFOAM scenarios.

In a particular case, we have also considered the liquid slug formation process at the pipe entrance with the superficial velocity condition of $v_{sg} = 2$ m.s⁻¹ and $v_{sl} = 0.2$ m.s⁻¹. From both the numerical simulations and the experimental observations presented in Fig. 8, one can see that a series of high frequency waves with small amplitude are propagated at the gas-liquid interface. After momentum transfer between gas and liquid in the slug flow regime, the wave frequency decreases while the amplitude increases. The pressure of gas gradu-

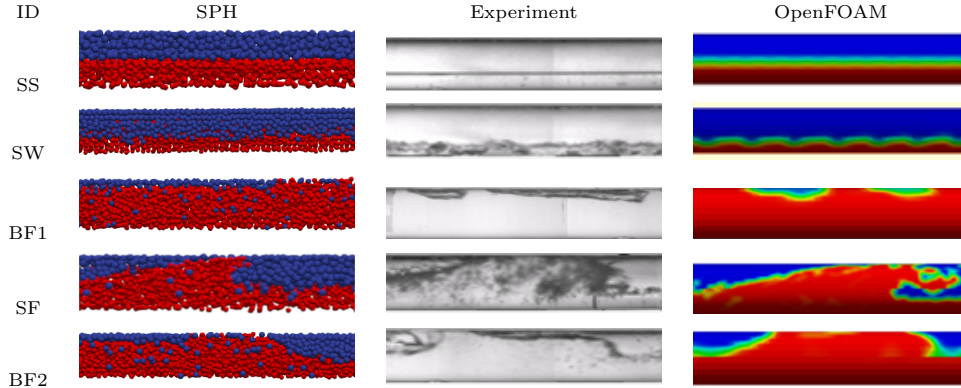


Figure 7: Gas-liquid multi-phase flow in a horizontal pipe: Flow patterns obtained by the presented SPH method in 3-D under various velocity conditions in comparison to the experimental and OpenFOAM simulations carried out by Wu et al. [20]. The velocity condition and flow pattern description of the above flow regimes are summarized in Table 2 denoted by the assigned ID.

ally drops due to the Bernoulli effect and the pressure difference between gas and liquid dominates the tension and gravity forces at the gas-liquid interface. Subsequently, the slug formation process initiates at the interface and the first liquid slug occurs at the entrance of the pipe.

Due to the prohibitive computational cost of 3-D simulations, both SPH and OpenFOAM simulations are carried out in 2-D in Fig. 8. The SPH simulation demonstrates a slightly lagged prediction of the slug formation, which is attributed to the turbulence model uncertainties that are not present in our methodology influencing the momentum exchange between gas and liquid. As discussed in Section 1, Ting et al. [38] and Ghasemi et al. [36] observed similar shortcomings when a 2-D SPH scheme was employed for a turbulent flow. Apart from this observation, the overall slug formation process and the pre-slug high frequency waves have been well predicted by the presented method.

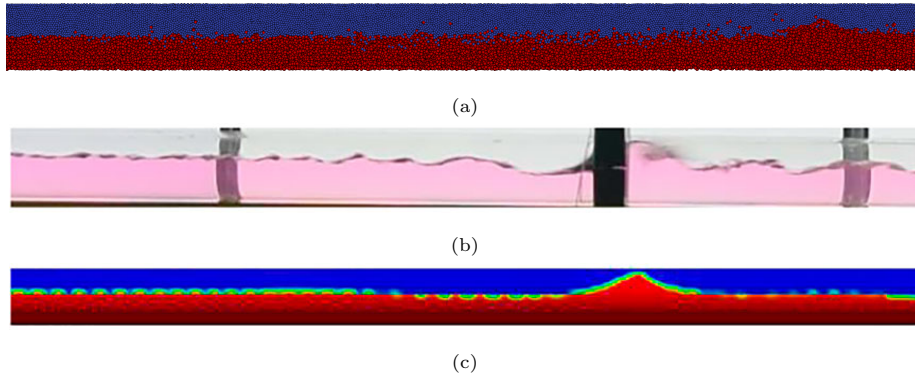


Figure 8: Gas-liquid multi-phase flow in a horizontal pipe: Slug formation process at the entrance of the pipe obtained by (a) SPH, (b) experiments and (c) OpenFOAM. Both the experimental and the OpenFOAM results are carried out by Wu et al.[20].

4. Numerical results and discussion

In this section, we present the obtained numerical results for various aspects of the slug flow in detail and discuss the insights gained by means of the presented 3-D computational framework based on SPH. The slug flow investigated herein owns the same configuration as depicted in Fig. 6.

Fig. 9 shows time series of slug development with the superficial velocity condition of $v_{sg} = 3 \text{ m.s}^{-1}$ and $v_{sl} = 1 \text{ m.s}^{-1}$. As it is observed, the first interaction of the high velocity gas with the slower liquid occurs at $t = 0.05 \text{ s}$ (Fig. 9b). We will investigate this moment later in-depth considering velocity vectors of the both phases. Meanwhile, one can note that from this point the momentum exchange between the phases accelerates and the first slug starts rising. At $t = 0.15 \text{ s}$ (Fig. 9d), the head of the slug has already jumped forward, which later at $t = 0.2 \text{ s}$ (Fig. 9e) falls under the effect of the gravity acceleration. Throughout the slug development, and in particular as the slug has passed by, low frequency waves with large amplitude are randomly generated due to the interfacial momentum transfer. It is also observed that slug roll-over happens, e.g., in Fig. 9d, which almost closes the channel. Similar observations have been reported also previously in the literature (see e.g., [18, 20, 40]).

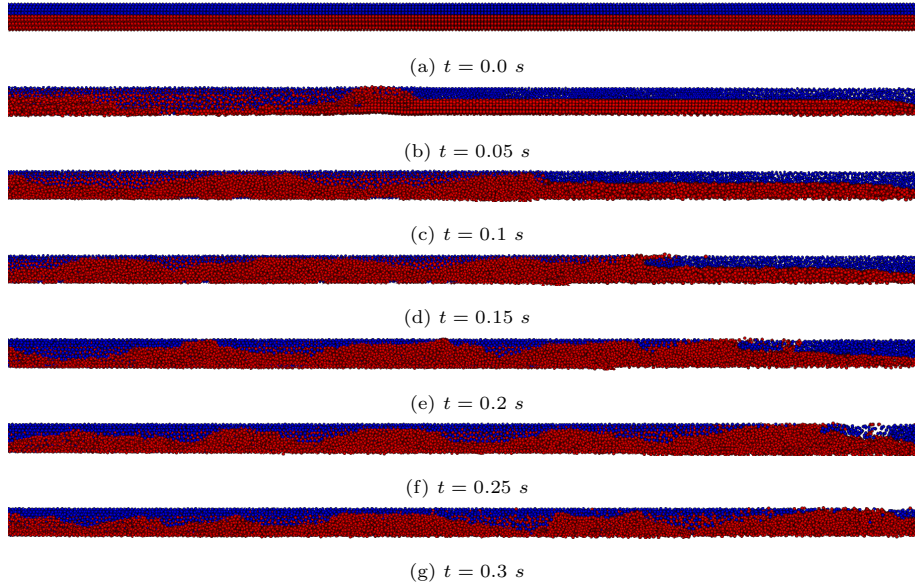


Figure 9: Gas-liquid multi-phase flow in a horizontal pipe: Time series of slug development with the superficial velocity condition of $v_{sg} = 3 \text{ m.s}^{-1}$ and $v_{sl} = 1 \text{ m.s}^{-1}$.

Figs. 10a and 10b show particle distribution together with pressure and velocity distribution, respectively, obtained by the presented method. It is noted that a quite smooth distribution of particles is achieved and pressure and velocity present no non-physical behavior, while differences in the pressure gradient at the phase interface are notable. As the slugging phenomena is driven by the gas pressure, a notable pressure gradient is also noted at the air-water interface. Consequently, the upper part of the liquid particles at the top of the slug are violently driven, which causes the slug roll-over, shown in Fig. 10b as the high velocity zone.

In order to further investigate the momentum exchange process causing the initiation of the first slug, Fig. 11 presents a zoom-in view of the first interaction between the high-velocity gas and the low-velocity liquid. In this figure, the solid yellow arrows represent the velocity vectors of the gas particles and the arrows scaled with their velocity values are the liquid particles velocity vectors. The length of the vectors also represents the magnitude of velocity at that point.

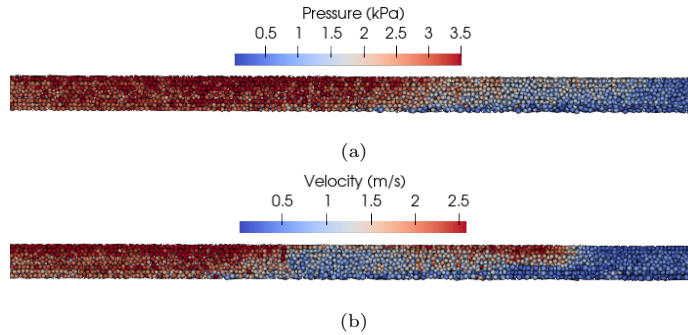


Figure 10: Gas-liquid multi-phase flow in a horizontal pipe: Particle distribution together with (a) pressure and (b) velocity distribution.

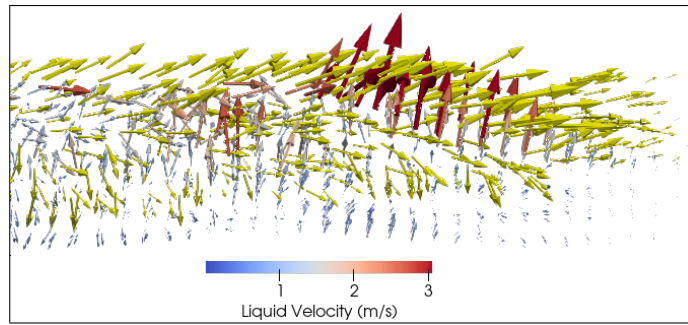


Figure 11: Gas-liquid multi-phase flow in a horizontal pipe: Zoom-in view of the velocity vectors of both gas (in solid yellow) and liquid (scaled by their velocity magnitude) particles at $t = 0.05$ s.

As it can be seen, the interfacial interaction between gas and liquid gives rise to the velocity of the liquid (red arrows) and causes a fully non-linear velocity distribution. Within the lower levels of liquid, on the contrary, the velocity magnitude is at its minimum as it has also been observed in Fig. 10b. As it can be also observed here, while the higher level air particles still have a relatively high velocity, its lower level particles have already lost their high kinetic energy due to the momentum exchange with liquid. The complex flow structures at this time instant are also remarkable.

The above reflections from the initiation of the first slug can be followed-up in Fig. 12. The figure plots the transient pressure signals recorded at the

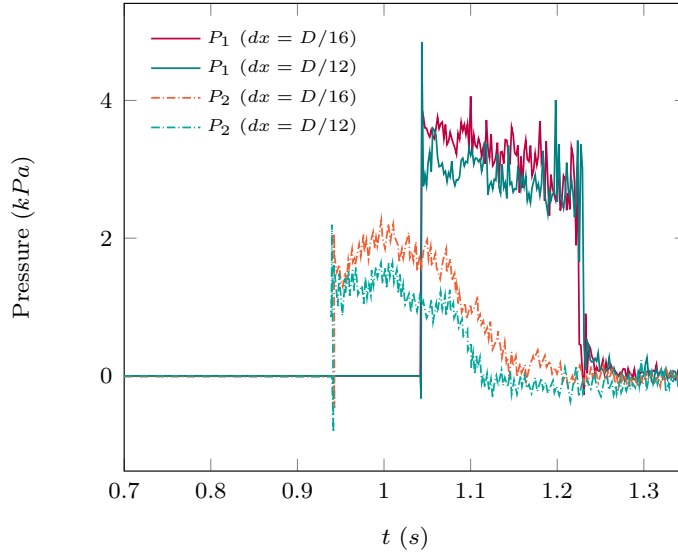


Figure 12: Gas-liquid multi-phase flow in a horizontal pipe: Transient pressure signals obtained at P_1 and P_2 sensors described in Fig. 6 for the velocity condition of $v_{sg} = 5 \text{ m.s}^{-1}$ and $v_{sl} = 1 \text{ m.s}^{-1}$.

two sensors shown in Fig. 6, P_1 and P_2 . As expected, an abrupt pressure increase has been recorded due to the rise of the first slug at both sensors. The duration of the rise time depends on the position of sensors at the pipe and the fact that whether the slug is developing or it is already developed. As the SPH formulations are in a weakly compressible framework, the pressure profile exhibits high frequency oscillations. It is worth noting that the measured pressure is obtained by averaging the values from particles within a support radius of $2.6dx$ [30].

It is possible to evaluate the rate of development of the slugs by analyzing the cross-sectional velocity profile along the pipe. Fig. 13 shows the velocity profiles at two different sections of the pipe, each being measured by means of three sequential probes placed with small distances after each other with the superficial velocity condition of $v_{sg} = 3 \text{ m.s}^{-1}$ and $v_{sl} = 1 \text{ m.s}^{-1}$. It can be observed in Fig. 13a that during the slug development the velocity of the liquid particles in higher vertical positions gradually increases along the slug

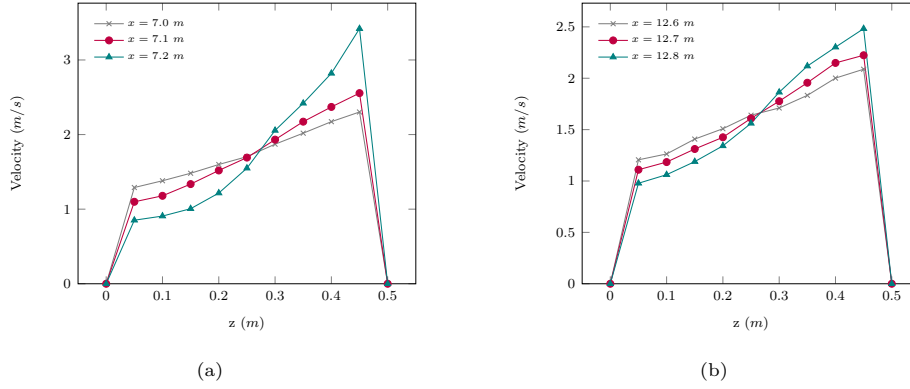


Figure 13: Gas-liquid multi-phase flow in a horizontal pipe: Velocity profile obtained for (a) developing and (b) developed slug with the velocity condition of $v_{sg} = 3 \text{ m.s}^{-1}$ and $v_{sl} = 1 \text{ m.s}^{-1}$.

length, whereas the velocity of the lower particles gradually drops. A similar velocity variation is noted between upper and lower parts of the liquid slug, in particular at $x = 7.2 \text{ m}$, where the slug has already been initiated and its head demonstrates a high velocity as observed also in Figs. 10b and 11. The velocity difference between upper and lower particles is mitigated in Fig. 13b, where the slug is fully developed.

Another important characteristic quantity of liquid slugging is the slug frequency, f_s , being defined as the inverse of the slug period, T , which is the time that a slug unit needs to pass through a measuring device

$$f_s = \frac{1}{T}. \quad (21)$$

Due to the prohibitive computational cost that impedes high resolution simulations, correctly detecting the slug head and tail to measure the slug period is not trivial. In this work we use the following formulation to measure an averaged slug frequency

$$\bar{f}_s = \frac{\sum_{i=1}^N f_{si}}{N} \quad (22)$$

where N is the number of times that the pressure sensors detect an abrupt pressure peak denoting a traveling slug. We placed ten pressure sensors along

the pipe to detect the head and tail of a traveling slug by measuring the time between two different pressure peaks. Fig. 14 plots the obtained slug frequencies along the pipe in comparison with the numerical and experimental results of Wu et al. [20] for the velocity condition of $v_{sg} = 3 \text{ m.s}^{-1}$ and $v_{sl} = 1 \text{ m.s}^{-1}$. The slug frequency evidently decreases as the slug travels away from the pipe entrance where the dense and light fluids are injected into the pipe with maximum velocity. The overall profile of the slug frequency has been well predicted with the SPH method, however, there are discrepancies between the SPH results and the experimental and numerical results of Wu et al. SPH demonstrates a delayed rise of frequency, which is consistent with the lagged slug initiation presented in Fig. 8a, although the computations related to Fig. 14 have been carried out in 3-D. The delayed slug formation, as discussed in Section 3.2, is attributed to the turbulence model uncertainties that influence the momentum exchange between gas and liquid, as well as the relatively coarse resolution dictated by the computational expenses. Finer resolution will demand a massively parallel framework as already presented by Rezavand et al. [42] and will be the scope of future developments. The SPH and OpenFOAM simulations used almost the same numerical resolution ($dx = D/16$), however, a higher rate of convergence is typically proven for the finite volume method (FVM) than that of SPH presented in Fig. 3b [60].

5. Conclusions

In this paper, we have numerically studied two-phase intermittent flows in a horizontal pipe and particularly focused on the slug flow regime. With the particle interactions being handled by a multi-phase SPH formulation based on a Riemann solver, the scheme is simple and the whole framework is not dependent on any empirical correlation for the slug flow.

Whilst a few studies have performed 3-D simulations of slug flow with commercial packages or computationally expensive methods, e.g., DNS, the present study presents the first Lagrangian 3-D description of the slug flows. The ob-

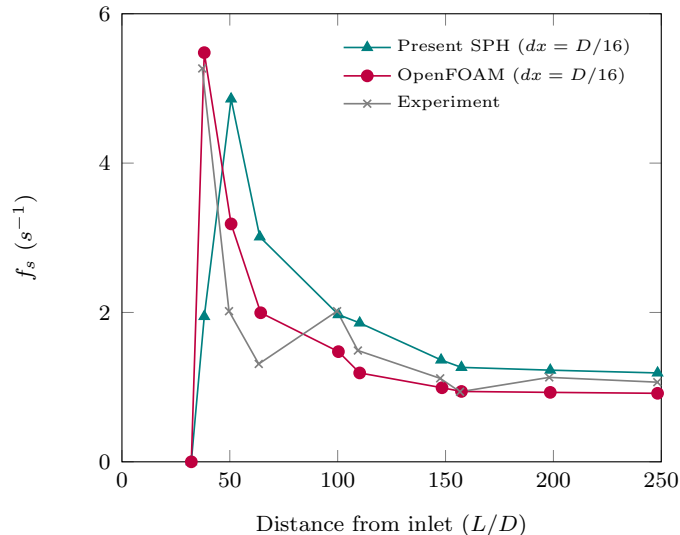


Figure 14: Gas-liquid multi-phase flow in a horizontal pipe: Slug frequency along the flow direction obtained by the presented SPH method in comparison with experimental observations and OpenFOAM simulations [20].

tained results show that the mesh-free formulation makes it possible to explicitly realize the interfacial interactions between gas and liquid, with no need for an interface tracking technique. The peculiarities of SPH in dealing with multi-phase phenomena facilitate the simulation of complex two-phase pipe flows.

The proposed method is validated against existing experimental data for some aspects of the slug flow regime and the results are verified in comparison with numerical and analytical solutions, as well, demonstrating reasonable agreements. 3-D description of the flow provides a more realistic representation of the studied real-world pipe flow.

Albeit the present work focuses on benchmark test cases, the method is sufficiently generic to be employed in more complex industrial applications. This will demand a massively parallel numerical framework, which is the main scope of the future developments. It is envisaged that the presented Lagrangian assets of SPH can improve the numerical analysis of slug flows to achieve a better design of pipeline systems concerning safety measures.

Acknowledgments

The authors gratefully acknowledge the financial support by Deutsche Forschungsgemeinschaft (DFG HU1572/10-1, DFG HU1527/12-4) for the present work. The authors also would like to thank Zhaoting Wang and colleagues for providing their experimental and numerical results for validation purposes.

References

References

- [1] A. Sausen, P. Sausen, M. de Campos, The slug flow problem in oil industry and pi level control, *New technologies in the oil and gas industry* (2012) 103–118.
- [2] W. Kirsner, Condensation-Induced Water Hammer in District Steam Systems: Circumstances Resulting in Catastrophic Failures Volume 4: Fluid Structure Interaction (2005) 875–881. [arXiv:https://asmedigitalcollection.asme.org/PVP/proceedings-pdf/PVP2005/41898/875/4560183/875\1.pdf](https://asmedigitalcollection.asme.org/PVP/proceedings-pdf/PVP2005/41898/875/4560183/875\1.pdf), doi:10.1115/PVP2005-71590. URL <https://doi.org/10.1115/PVP2005-71590>
- [3] M. Bonizzi, Transient one-dimensional modelling of multiphase slug flows, Ph.D. thesis, Imperial College London (University of London) (2003).
- [4] J. Fabre, A. Line, Modeling of two-phase slug flow, *Annual Review of Fluid Mechanics* 24 (1) (1992) 21–46. [arXiv:https://doi.org/10.1146/annurev.fl.24.010192.000321](https://doi.org/10.1146/annurev.fl.24.010192.000321), doi:10.1146/annurev.fl.24.010192.000321. URL <https://doi.org/10.1146/annurev.fl.24.010192.000321>
- [5] P. M. Ujang, Studies of slug initiation and development in two-phase gas-liquid pipeline flow, Ph.D. thesis, Imperial College London (University of London) (2003).

- [6] J. Mandhane, G. Gregory, K. Aziz, A flow pattern map for gas—liquid flow in horizontal pipes, *International journal of multiphase flow* 1 (4) (1974) 537–553.
- [7] K. Mishima, M. Ishii, Theoretical Prediction of Onset of Horizontal Slug Flow, *Journal of Fluids Engineering* 102 (4) (1980) 441–445. [arXiv:https://asmedigitalcollection.asme.org/fluidsengineering/article-pdf/102/4/441/5531529/441_1.pdf](https://asmedigitalcollection.asme.org/fluidsengineering/article-pdf/102/4/441/5531529/441_1.pdf), doi:10.1115/1.3240720. URL <https://doi.org/10.1115/1.3240720>
- [8] D. Barnea, A unified model for predicting flow-pattern transitions for the whole range of pipe inclinations, *International journal of multiphase flow* 13 (1) (1987) 1–12.
- [9] Y. Taitel, A. E. Dukler, A model for predicting flow regime transitions in horizontal and near horizontal gas-liquid flow, *AIChE journal* 22 (1) (1976) 47–55.
- [10] G. Lerchl, H. Austregesilo, A. Langenfeld, P. J. Schoeffel, D. von der Cron, F. Weyermann, *Athlet 3.2 - user's manual*, Tech. rep., GRS, GRS-P-1/ Vol. 1 Rev.8 (2019).
- [11] B. D. Chung, K. D. Kim, S. W. Bae, J. J. Jeong, S. W. Lee, M. K. Hwang, C. Yoon, *Mars code manual volume i: code structure, system models, and solution methods*, Tech. rep., Korea Atomic Energy Research Institute (2010).
- [12] S. Bajorek, et al., *Trace v5. 0 theory manual, Field Equations, Solution Methods and Physical Models*, US Nuclear Regulatory Commission (2008).
- [13] F. Bloemeling, T. Neuhaus, A. Schaffrath, 1d models for condensation induced water hammer in pipelines, *Kerntechnik* 78 (1) (2013) 31–34 [cited 2023-02-19]. doi:doi:10.3139/124.110308. URL <https://doi.org/10.3139/124.110308>

- [14] J. Lee, M. Junk, T. Skorek, P. Josef Schöffel, Improvement of entrainment model for horizontal flow in athlet and application to mantilla experiment and tptf, *Nuclear Engineering and Design* 400 (2022) 112066. doi:<https://doi.org/10.1016/j.nucengdes.2022.112066>.
URL <https://www.sciencedirect.com/science/article/pii/S0029549322004174>
- [15] M. Ishii, Thermo-fluid dynamic theory of two-phase flow, NASA Sti/recon Technical Report A 75 (1975) 29657.
- [16] M. Lu, Experimental and computational study of two-phase slug flow, Ph.D. thesis, Imperial College London UK (2015).
- [17] S. P. Korzilius, A. S. Tijsseling, Z. Bozkuş, M. J. Anthonissen, W. H. Schilders, Modeling liquid slugs accelerating in inclined conduits, *Journal of Pressure Vessel Technology* 139 (6) (2017).
- [18] C. Vallée, T. Höhne, H.-M. Prasser, T. Sühnel, Experimental investigation and cfd simulation of horizontal stratified two-phase flow phenomena, *Nuclear Engineering and Design* 238 (3) (2008) 637–646.
- [19] M. Abdulkadir, V. Hernandez-Perez, I. Lowndes, B. Azzopardi, E. Sambomah, Experimental study of the hydrodynamic behaviour of slug flow in a horizontal pipe, *Chemical Engineering Science* 156 (2016) 147–161. doi:<https://doi.org/10.1016/j.ces.2016.09.015>.
URL <https://www.sciencedirect.com/science/article/pii/S0009250916304948>
- [20] X. Wu, Z. Wang, M. Dong, Q. Ge, L. Dong, Simulation study on the development process and phase interface structure of gas-liquid slug flow in a horizontal pipe, *Frontiers in Energy Research* 9 (2021). doi:[10.3389/fenrg.2021.762471](https://doi.org/10.3389/fenrg.2021.762471).
URL <https://www.frontiersin.org/articles/10.3389/fenrg.2021.762471>

- [21] M. Ramdin, R. Henkes, Computational fluid dynamics modeling of benjamin and taylor bubbles in two-phase flow in pipes, *Journal of fluids engineering* 134 (4) (2012).
- [22] T. Taha, Z. Cui, Hydrodynamics of slug flow inside capillaries, *Chemical Engineering Science* 59 (6) (2004) 1181–1190.
doi:<https://doi.org/10.1016/j.ces.2003.10.025>.
URL <https://www.sciencedirect.com/science/article/pii/S0009250903005979>
- [23] Z. I. Al-Hashimy, H. H. Al-Kayiem, R. W. Time, Z. K. Kadhim, Numerical characterisation of slug flow in horizontal air/water pipe flow, *International Journal of Computational Methods and Experimental Measurements* 4 (2) (2016) 114–130.
- [24] K. Fukagata, N. Kasagi, P. Ua-arayaporn, T. Himeno, Numerical simulation of gas–liquid two-phase flow and convective heat transfer in a micro tube, *International Journal of Heat and Fluid Flow* 28 (1) (2007) 72–82, the International Conference on Heat Transfer and Fluid Flow in Microscale (HTFFM-05).
doi:<https://doi.org/10.1016/j.ijheatfluidflow.2006.04.010>.
URL <https://www.sciencedirect.com/science/article/pii/S0142727X06001354>
- [25] Z. Yu, O. Hemminger, L.-S. Fan, Experiment and lattice boltzmann simulation of two-phase gas–liquid flows in microchannels, *Chemical Engineering Science* 62 (24) (2007) 7172–7183, 8th International Conference on Gas-Liquid and Gas-Liquid-Solid Reactor Engineering.
doi:<https://doi.org/10.1016/j.ces.2007.08.075>.
URL <https://www.sciencedirect.com/science/article/pii/S0009250907006884>
- [26] F. Xie, X. Zheng, M. S. Triantafyllou, Y. Constantinides, Y. Zheng, G. Em Karniadakis, Direct numerical simulations of two-phase flow in

- an inclined pipe, *Journal of Fluid Mechanics* 825 (2017) 189–207. doi: 10.1017/jfm.2017.417.
- [27] M. Rezavand, M. Taeibi-Rahni, W. Rauch, An ISPH scheme for numerical simulation of multiphase flows with complex interfaces and high density ratios, *Comput. Math. Appl.* 75 (8) (2018) 2658–2677. doi:10.1016/j.camwa.2017.12.034.
- [28] X. Su, M. Luo, X. Zhao, A. Khayyer, Oil Spill Spreading Simulation Based on an Enhanced Multi-phase Consistent Particle Method, *International Journal of Offshore and Polar Engineering* 32 (04) (2022) 377–385. arXiv:<https://onepetro.org/IJ0PE/article-pdf/32/04/377/3055546/isope-22-32-4-377.pdf>, doi:10.17736/ijope.2022.jc873. URL <https://doi.org/10.17736/ijope.2022.jc873>
- [29] E. A. Patiño-Nariño, A. F. Galvis, R. Pavanello, M. R. Gongora-Rubio, Modeling of co-axial bubbles coalescence under moderate reynolds regimes: A bi-phase sph approach, *International Journal of Multiphase Flow* 162 (2023) 104355. doi:<https://doi.org/10.1016/j.ijmultiphaseflow.2022.104355>. URL <https://www.sciencedirect.com/science/article/pii/S0301932222003147>
- [30] M. Rezavand, C. Zhang, X. Hu, A weakly compressible sph method for violent multi-phase flows with high density ratio, *Journal of Computational Physics* 402 (2020) 109092. doi:<https://doi.org/10.1016/j.jcp.2019.109092>. URL <https://www.sciencedirect.com/science/article/pii/S0021999119307971>
- [31] C. Zhang, M. Rezavand, Y. Zhu, Y. Yu, D. Wu, W. Zhang, J. Wang, X. Hu, Sphinxsys: An open-source multi-physics and multi-resolution library based on smoothed particle hydrodynamics, *Computer Physics Communications* 267 (2021) 108066.

doi:<https://doi.org/10.1016/j.cpc.2021.108066>.

URL <https://www.sciencedirect.com/science/article/pii/S0010465521001788>

- [32] C. Zhang, J. Wang, M. Rezavand, D. Wu, X. Hu, An integrative smoothed particle hydrodynamics method for modeling cardiac function, *Computer Methods in Applied Mechanics and Engineering* 381 (2021) 113847. doi:<https://doi.org/10.1016/j.cma.2021.113847>.
URL <https://www.sciencedirect.com/science/article/pii/S0045782521001845>
- [33] A. Khayyer, Y. Shimizu, T. Gotoh, H. Gotoh, Enhanced resolution of the continuity equation in explicit weakly compressible sph simulations of incompressible free-surface fluid flows, *Applied Mathematical Modelling* 116 (2023) 84–121. doi:<https://doi.org/10.1016/j.apm.2022.10.037>.
URL <https://www.sciencedirect.com/science/article/pii/S0307904X22005091>
- [34] T. Douillet-Grellier, F. De Vuyst, H. Calandra, P. Ricoux, Simulations of intermittent two-phase flows in pipes using smoothed particle hydrodynamics, *Computers & Fluids* 177 (2018) 101–122. doi:<https://doi.org/10.1016/j.compfluid.2018.10.004>.
URL <https://www.sciencedirect.com/science/article/pii/S0045793018307199>
- [35] T. Douillet-Grellier, S. Leclaire, D. Vidal, F. Bertrand, F. De Vuyst, Comparison of multiphase sph and lbm approaches for the simulation of intermittent flows, *Computational Particle Mechanics* 6 (2019) 695–720.
- [36] A. Ghasemi V., B. Firoozabadi, M. Mahdinia, 2D numerical simulation of density currents using the SPH projection method, *Eur. J. Mech. B. Fluids* 38 (2013) 38–46. doi:[10.1016/j.euromechflu.2012.10.004](https://doi.org/10.1016/j.euromechflu.2012.10.004).
- [37] P. W. Cleary, J. J. Monaghan, Boundary interactions and transition to tur-

- bulence for standard cfd problems using sph, Proc. of the 6th International Computational Techniques and Applications (1993) 157–165.
- [38] T. S. Ting, M. Prakash, P. Cleary, M. Thompson, Simulation of high reynolds number flow over a backward facing step using sph, ANZIAM Journal 47 (2005) C292–C309.
- [39] R. Vacondio, C. Altomare, M. De Leffe, X. Hu, D. Le Touzé, S. Lind, J.-C. Marongiu, S. Marrone, B. D. Rogers, A. Souto-Iglesias, Grand challenges for smoothed particle hydrodynamics numerical schemes, Computational Particle Mechanics 8 (2021) 575–588.
- [40] A. O. Mohmmed, H. H. Al-Kayiem, A. Osman, Investigations on the slug two-phase flow in horizontal pipes: Past, presents, and future directives, Chemical Engineering Science 238 (2021) 116611. doi:<https://doi.org/10.1016/j.ces.2021.116611>.
URL <https://www.sciencedirect.com/science/article/pii/S0009250921001767>
- [41] C. Zhang, M. Rezavand, Y. Zhu, Y. Yu, D. Wu, W. Zhang, J. Wang, X. Hu, Sphinxsys: an open-source multi-physics and multi-resolution library based on smoothed particle hydrodynamics, Computer Physics Communications (2021) 108066doi:<https://doi.org/10.1016/j.cpc.2021.108066>.
- [42] M. Rezavand, C. Zhang, X. Hu, Generalized and efficient wall boundary condition treatment in gpu-accelerated smoothed particle hydrodynamics, Computer Physics Communications 281 (2022) 108507. doi:<https://doi.org/10.1016/j.cpc.2022.108507>.
URL <https://www.sciencedirect.com/science/article/pii/S0010465522002260>
- [43] J. J. Monaghan, Smoothed Particle Hydrodynamics and Its Diverse Applications, Annu. Rev. Fluid Mech. 44 (1) (2012) 323–346. doi:[10.1146/annurev-fluid-120710-101220](https://doi.org/10.1146/annurev-fluid-120710-101220).

- [44] J. Vila, On particle weighted methods and smooth particle hydrodynamics, *Math. Models Methods Appl. Sci.* 9 (02) (1999) 161–209. doi:<https://doi.org/10.1142/S0218202599000117>.
- [45] C. Zhang, X. Hu, N. A. Adams, A weakly compressible SPH method based on a low-dissipation Riemann solver, *J. Comput. Phys.* 335 (2017) 605–620. doi:<https://doi.org/10.1016/j.jcp.2017.01.027>.
- [46] X. Y. Hu, B. C. Khoo, An interface interaction method for compressible multifluids, *J. Comput. Phys.* 198 (1) (2004) 35–64. doi:[10.1016/j.jcp.2003.12.018](https://doi.org/10.1016/j.jcp.2003.12.018).
- [47] S. Adami, X. Hu, N. Adams, A generalized wall boundary condition for smoothed particle hydrodynamics, *J. Comput. Phys.* 231 (21) (2012) 7057–7075. doi:[10.1016/j.jcp.2012.05.005](https://doi.org/10.1016/j.jcp.2012.05.005).
- [48] S. Zhang, W. Zhang, C. Zhang, X. Hu, A lagrangian free-stream boundary condition for weakly compressible smoothed particle hydrodynamics (2022). doi:[10.48550/ARXIV.2206.06875](https://doi.org/10.48550/ARXIV.2206.06875).
URL <https://arxiv.org/abs/2206.06875>
- [49] M. Lastiwka, M. Basa, N. J. Quinlan, Permeable and non-reflecting boundary conditions in sph, *International Journal for Numerical Methods in Fluids* 61 (7) (2009) 709–724. arXiv:<https://onlinelibrary.wiley.com/doi/pdf/10.1002/flid.1971>, doi:<https://doi.org/10.1002/flid.1971>.
URL <https://onlinelibrary.wiley.com/doi/abs/10.1002/flid.1971>
- [50] J. J. Monaghan, Smoothed particle hydrodynamics, *Rep. Prog. Phys.* 68 (8) (2005) 1703.
URL <http://stacks.iop.org/0034-4885/68/i=8/a=R01>
- [51] S. Adami, X. Hu, N. A. Adams, A transport-velocity formulation for smoothed particle hydrodynamics, *J. Comput. Phys.* 241 (2013) 292–307. doi:[10.1016/j.jcp.2013.01.043](https://doi.org/10.1016/j.jcp.2013.01.043).

- [52] C. Zhang, M. Rezavand, X. Hu, Dual-criteria time stepping for weakly compressible smoothed particle hydrodynamics, *Journal of Computational Physics* 404 (2020) 109135. doi:<https://doi.org/10.1016/j.jcp.2019.109135>.
URL <https://www.sciencedirect.com/science/article/pii/S002199911930840X>
- [53] D. Wu, C. Zhang, X. Tang, X. Hu, An hourglass-free formulation for total lagrangian smoothed particle hydrodynamics (2022). doi:10.48550/ARXIV.2212.00753.
URL <https://arxiv.org/abs/2212.00753>
- [54] C. Zhang, M. Rezavand, X. Hu, A multi-resolution sph method for fluid-structure interactions, *Journal of Computational Physics* 429 (2021) 110028. doi:<https://doi.org/10.1016/j.jcp.2020.110028>.
URL <https://www.sciencedirect.com/science/article/pii/S0021999120308020>
- [55] Y. Ren, A. Khayyer, P. Lin, X. Hu, Numerical modeling of sloshing flow interaction with an elastic baffle using sphinxsys, *Ocean Engineering* 267 (2023) 113110. doi:<https://doi.org/10.1016/j.oceaneng.2022.113110>.
URL <https://www.sciencedirect.com/science/article/pii/S0029801822023939>
- [56] C. Zhang, Y. Zhu, Y. Yu, D. Wu, M. Rezavand, S. Shao, X. Hu, An artificial damping method for total lagrangian sph method with application in biomechanics, *Engineering Analysis with Boundary Elements* 143 (2022) 1–13. doi:<https://doi.org/10.1016/j.enganabound.2022.05.022>.
URL <https://www.sciencedirect.com/science/article/pii/S0955799722001783>
- [57] J. P. Morris, P. J. Fox, Y. Zhu, Modeling low reynolds number incompressible flows using sph, *Journal of Computational Physics* 136 (1) (1997)

214–226. doi:<https://doi.org/10.1006/jcph.1997.5776>.

URL <https://www.sciencedirect.com/science/article/pii/S0021999197957764>

- [58] R. B. Bird, W. E. Stewart, E. N. Lightfoot, *Transport phenomena*, New York: John Wiley & Sons, Inc, 2002.
- [59] R. Fatehi, M. Manzari, Error estimation in smoothed particle hydrodynamics and a new scheme for second derivatives, *Computers & Mathematics with Applications* 61 (2) (2011) 482–498. doi:10.1016/j.camwa.2010.11.028.
- [60] Z. Cai, On the finite volume element method, *Numerische Mathematik* 58 (1) (1990) 713–735.